Overwhelming O^+ contribution to the plasma sheet energy density during the October 2003 superstorm: Geotail/EPIC and IMAGE/LENA observations

M. Nosé,[1] S. Taguchi,[2] K. Hosokawa,[2] S. P. Christon,[3] R. W. McEntire,[4] T. E. Moore,[5] and M. R. Collier[5]

Received 30 November 2004; revised 10 March 2005; accepted 28 April 2005; published 25 August 2005.

[1] We studied dynamics of O^+ ions during the superstorm that occurred on 29–31 October 2003, using energetic (9–210 keV/*e*) ion flux data obtained by the energetic particle and ion composition (EPIC) instrument on board the Geotail satellite and neutral atom data in the energy range of 10 eV to a few keV acquired by the low-energy neutral atom (LENA) imager on board the Imager for Magnetopause-to-Aurora Global Exploration (IMAGE) satellite. Since the low-energy neutral atoms are created from the outflowing ionospheric ions by the charge exchange process, we could examine variations of ionospheric ion outflow with the IMAGE/LENA data. In the near-Earth plasma sheet of $X_{GSM} \sim -6\ R_E$ to $-8.5\ R_E$, we found that the H^+ energy density showed no distinctive differences between the superstorm and quiet intervals (1–10 keV cm^{-3}), while the O^+ energy density increased from 0.05–3 keV cm^{-3} during the quiet intervals to ~100 keV cm^{-3} during the superstorm. The O^+/H^+ energy density ratio reached 10–20 near the storm maximum, which is the largest ratio in the near-Earth plasma sheet ever observed by Geotail, indicating more than 90% of O^+ in the total energy density. We argued that such extreme increase of the O^+/H^+ energy density ratio during the October 2003 superstorm was due to mass-dependent acceleration of ions by storm-time substorms as well as an additional supply of O^+ ions from the ionosphere to the plasma sheet. We compared the ion composition between the ring current and the near-Earth plasma sheet reported by previous studies and found that they are rather similar. On the basis of the similarity, we estimated that the ring current had the O^+/H^+ energy density ratio as large as 10–20 for the October 2003 superstorm.

Citation: Nosé, M., S. Taguchi, K. Hosokawa, S. P. Christon, R. W. McEntire, T. E. Moore, and M. R. Collier (2005), Overwhelming O^+ contribution to the plasma sheet energy density during the October 2003 superstorm: Geotail/EPIC and IMAGE/LENA observations, *J. Geophys. Res.*, *110*, A09S24, doi:10.1029/2004JA010930.

1. Introduction

[2] An extremely intense geomagnetic storm occurred on 29–31 October 2003. This storm was initiated by a sudden commencement at 0612 UT on 29 October, as can be seen in the SYM-H index (Figure 1), which is almost equivalent to the 1-min Dst index [*Iyemori et al.*, 1992]. The SYM-H index showed two local minima in the middle of 29 October and in the beginning of 30 October, followed by the minimum at 2255 UT on 30 October with the value of −432 nT. Around the time of minimum of SYM-H (SYM-H_{min}), the Geotail satellite was located in the near-Earth geomagnetic tail ($X_{GSM} \sim -6\ R_E$ to $-8.5\ R_E$) and the Imager for Magnetopause-to-Aurora Global Exploration (IMAGE) satellite was on the morningside. The Geotail satellite carried the energetic particle and ion composition (EPIC) instrument that can measure energetic (9–210 keV/*e*) ion flux with mass and charge state information; the IMAGE satellite carried the low-energy neutral atom (LENA) imager that can detect neutral atoms of 10 eV to a few keV generated by charge exchange with ionospheric outflow ions. In this study we studied how energetic ion composition in the near-Earth plasma sheet was changing during the October 2003 superstorm and how the ion composition change was related to ionospheric ion outflow, using both the Geotail/EPIC data and the IMAGE/LENA data.

[3] It has been reported by a large number of previous studies that ion composition in the ring current changes

[1]Data Analysis Center for Geomagnetism and Space Magnetism, Graduate School of Science, Kyoto University, Kyoto, Japan.
[2]Department of Information and Communication Engineering, University of Electro-Communications, Tokyo, Japan.
[3]Focused Analysis and Research, Columbia, Maryland, USA.
[4]Applied Physics Laboratory, Johns Hopkins University, Laurel, Maryland, USA.
[5]NASA Goddard Space Flight Center, Greenbelt, Maryland, USA.

0148-0227/05/2004JA010930$09.00

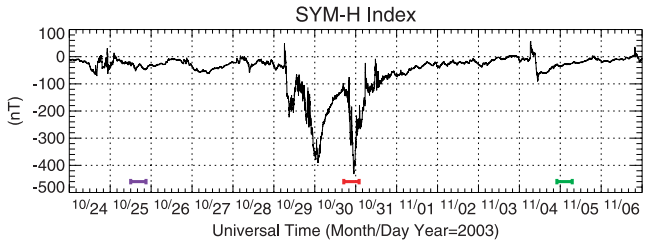

Figure 1. The SYM-H index for the October 2003 superstorm. Horizontal bars indicate the time intervals when the Geotail/EPIC data were analyzed. The blue bar is from 1200–2100 UT on 25 October, the red bar is from 1700 UT on 30 October to 0200 UT on 31 October, and the green bar is from 2200 UT on 4 November to 0700 UT on 5 November.

drastically during magnetic storms [*Gloeckler et al.*, 1985; *Krimigis et al.*, 1985; *Hamilton et al.*, 1988; *Roeder et al.*, 1996; *Daglis*, 1997; *Daglis et al.*, 2000; *Feldstein et al.*, 2000; *Greenspan and Hamilton*, 2002]. *Roeder et al.* [1996] and *Daglis* [1997] reported that the O^+/H^+ energy density ratio reached to even 2–3 for the large magnetic storm with minimum of Dst of −298 nT which occurred on 23 March 1991. It is of great interest to examine the O^+/H^+ energy density ratio in this superstorm (SYM-H_{min} = −432 nT). However, no satellites made in situ observations of ion composition in the inner magnetosphere during this event. We used the Geotail observation in the plasma sheet to estimate the O^+/H^+ ratio in the ring current because the plasma in the near-Earth plasma sheet is considered as a direct source of the ring current plasma.

[4] The organization of this paper is as follows. In section 2 we describe the Geotail and IMAGE data used in this study. We selected three time intervals for analysis, one of which is the superstorm interval and two of which are quiet intervals (i.e., intervals before and after the superstorm). In section 3 observations with the Geotail/EPIC and IMAGE/LENA instruments are shown. It was found that the O^+/H^+ energy density ratio during the superstorm had the largest value in the Geotail observations of the near-Earth plasma sheet (X_{GSM} = −10 R_E to 0 R_E and $|Y_{GSM}| \leq 8$ R_E) till the end of 2003. (Before the superstorm occurs, the largest ratio in the near-Earth plasma sheet observed by Geotail was 3–4.5 during the storm of 5 October 2000.) Increases of the O^+/H^+ energy density ratio were associated with storm-time substorms and ion outflow from the ionosphere. In section 4 we discuss dynamics of O^+ ions during the superstorm and estimate the ring current ion composition from the Geotail measurement. The conclusions are given in section 5.

2. Instrumentation and Data Set

2.1. Geotail and IMAGE Satellites

[5] The Geotail satellite was launched on 24 July 1992 [*Nishida*, 1994]. In October 2003 the satellite was in the near-Earth orbit having a perigee of ∼9 R_E, an apogee of ∼30 R_E, an inclination of ∼−9.5°, and an orbital period of ∼125 hours. The EPIC instrument on board the Geotail satellite is composed of two separate sensors, the suprathermal ion composition spectrometer (STICS) and the ion composition subsystem (ICS) [*Williams et al.*, 1994]. In this study we utilized data from the STICS sensor that measures differential fluxes of H^+ and O^+ ions with energy range of 9–210 keV/*e* in eight logarithmically spaced energy steps. Spatial coverage of the STICS sensor is almost 4π sr. One complete energy spectrum is provided in a time resolution of ∼24 s. From each energy spectrum we calculated energy densities of H^+ and O^+ ions in the same way as that by *Nosé et al.* [2001, 2003]. Then the calculated H^+ and O^+ energy densities were averaged over 5 min, which are used in the following analysis. The magnetic field data acquired by the magnetic field (MGF) experiment on board Geotail were also examined [*Kokubun et al.*, 1994]. Time resolution of the MGF data used here is 1 min.

[6] The IMAGE satellite was launched into a polar orbit with a perigee of 1000 km altitude and an apogee of 8.2 R_E on 25 March 2000 [*Burch*, 2000]. Its orbital period is 14.2 hours. The satellite spins in the reverse cartwheel mode; that is, the spin vector is antiparallel to the orbital momentum vector. The LENA instrument on board the IMAGE satellite was designed to measure neutral atoms in the energy range of ∼10 eV to a few keV with mass information [*Moore et al.*, 2000]. The neutral atoms incoming to the instrument hit a tungsten conversion surface at grazing incidence, where a small fraction of them is converted to negative ions. Then the negative ions are detected by the electrostatic analyzer and the time-of-flight mass spectrometer. It has been reported that energetic neutral O hitting the tungsten conversion surface can sputter O^- and H^- and that energetic neutral H at energies above ∼300 eV can sputter H^- and O^- from the surface as well [*Moore et al.*, 2000; *Collier et al.*, 2001; *Khan et al.*, 2003]. This feature makes it complicated to determine the composition of the incident neutral atoms from the observed time-of-flight spectrum. Thus we used data combining the H and O peaks in the time-of-flight spectrum. A field of view of the LENA instrument spans ±45° against a plane perpendicular to the satellite spin axis and it is divided by 12 polar sectors. As the satellite spins, the instrument sweeps out 360° in azimuth direction, which is divided by 45 azimuthal sectors. One complete image covering an area of 90° (polar) × 360° (azimuth) is obtained over one spin period (2 min) with 12 × 45 pixels, each of which has a ∼8° × 8° angular resolution. In the following analysis we used data averaged over the 12 polar sectors, that is, azimuthally binned data.

2.2. Time Interval for Analysis

[7] We selected a time interval of 1700 UT on 30 October to 0200 UT on 31 October for analysis, which is indicated by a horizontal red bar in the bottom of Figure 1. Note that the red bar covers the SYM-H_{min}. The Geotail orbit during this 9-hour time interval is indicated with a red line in Figure 2. Red dots on the line designate the locations of Geotail every 1 hour. In this time interval Geotail surveyed the near-Earth region of X_{GSM} = −6 R_E to −8.5 R_E.

[8] We also examined the ion composition during intervals that are separated by one Geotail orbital period (about 125 hours) from the aforementioned storm interval. These intervals are shown with blue and green bars in the bottom of Figure 1; the blue bar is from 1200–2100 UT on 25 October (before the superstorm) and the green bar is from 2200 UT on 4 November to 0700 UT on 5 November (after

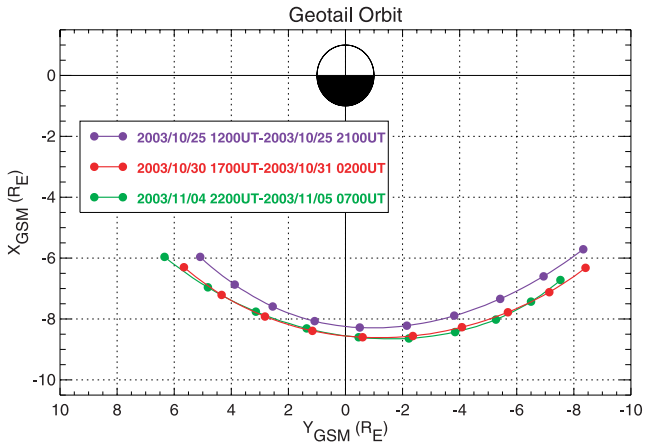

Figure 2. Geotail orbits in the equatorial plane during the superstorm (red) and the quiet intervals (blue and green). Time intervals correspond to those shown in Figure 1 with the same color. Dots on the orbits show the locations of Geotail every 1 hour.

the superstorm). The SYM-H index in the former interval shows only slight variations. The latter interval is in the recovery phase of a moderate magnetic storm that started in the beginning of 4 November. The SYM-H index throughout these intervals was mostly −30 nT to −40 nT. We refer these intervals as quiet intervals thereafter because SYM-H of −30 nT to −40 nT is much larger than SYM-H_{min} of −432 nT. Geotail orbits for these quiet intervals are shown in Figure 2 with corresponding colors. It should be noted that Geotail surveyed the nearly same area in both the storm (red) and quiet (blue and green) intervals.

3. Observations

3.1. Plasma Sheet Ion Composition Observed by Geotail/EPIC/STICS

[9] Figure 3 compiles the SYM-H index as well as the Geotail/EPIC and Geotail/MGF data. Figure 3a is the SYM-H index, and Figures 3b–3e give the H^+ energy density, the O^+ energy density, the magnetic field in the X_{GSM} component, and the O^+/H^+ energy density ratio, respectively. In each panel we plotted data of the storm and quiet intervals (i.e., the three 9-hour intervals stated above). Different colors mean different intervals, that is, red for the storm interval, blue for the former quiet interval, and green for the latter quiet interval. (Unfortunately, Geotail had no measurements from 2200 UT on 4 November to 0040 UT on 5 November.) This style of data presentation makes it easy for us to compare the Geotail data in the almost same area of the near-Earth tail between different geomagnetic conditions, as can be understood from Figure 2.

[10] The SYM-H index shown with red color decreased gradually from −100 nT to the minimum, followed by a recovery to about −250 nT. The blue and green traces of the SYM-H index stayed at the level of −30 nT to −40 nT. From Figure 3b we notice that the H^+ energy density in the storm interval was 1–10 keV cm^{-3} and those in the quiet intervals were 0.5–10 keV cm^{-3}. There were no significant differences in the H^+ energy density among the three intervals. However, the O^+ energy density in the storm interval was much larger than those in the quiet intervals (Figure 3c). The O^+ energy density gradually increased from 1 keV cm^{-3} to 100 keV cm^{-3} as the magnetic storm developed and then decreased to 10 keV cm^{-3} by 0200 UT on 31 October. In the former and latter quiet intervals (blue and green), the O^+ energy density was 0.1–3 keV cm^{-3} and 0.05–1 keV cm^{-3}, respectively. The magnetic field in the X component plotted in Figure 3d indicates that the locations of Geotail relative to the current sheet were variable, in particular, during the storm interval. Thus the energy density may contain a spatial effect. For example, from

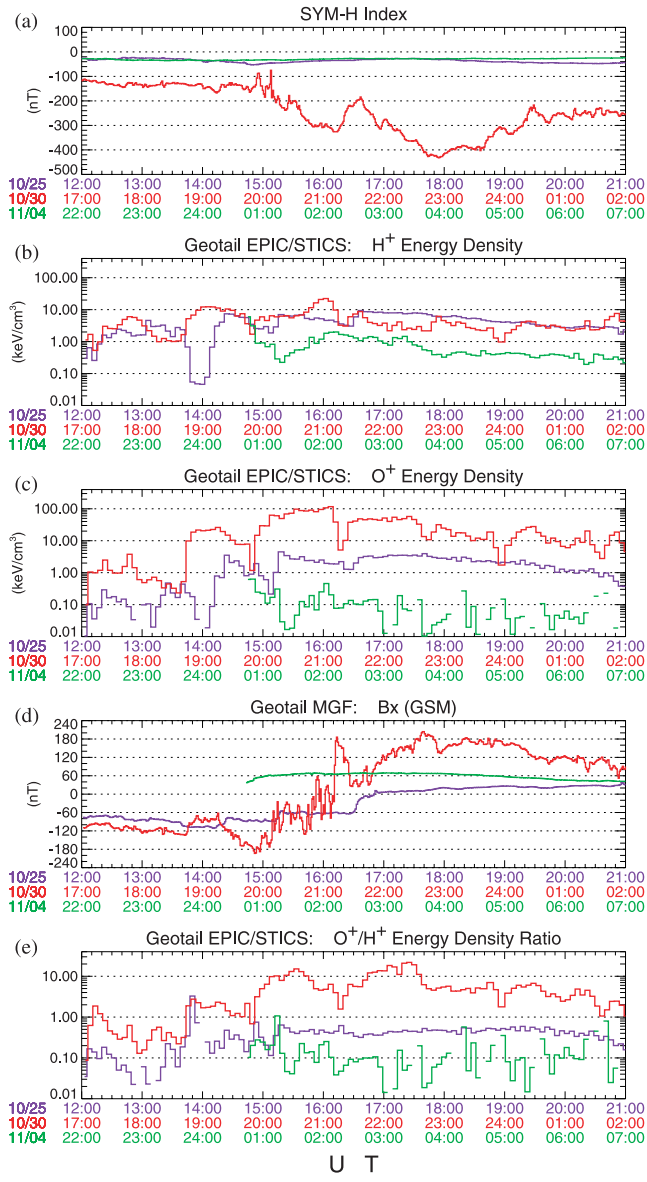

Figure 3. From top to bottom: (a) the SYM-H index; (b) the H^+ energy density and (c) the O^+ energy density calculated from the Geotail/EPIC/STICS data; (d) the X component of the magnetic field measured by Geotail/MGF; and (e) the O^+/H^+ energy density ratio from Geotail/EPIC/STICS. Different colors represent different time intervals, as same as in Figures 1 and 2.

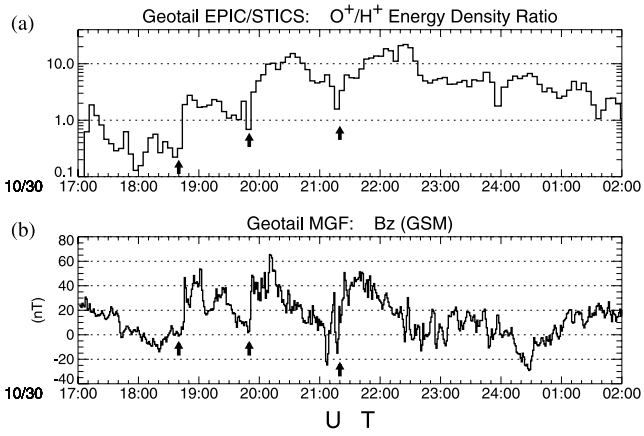

Figure 4. (a) The O^+/H^+ energy density ratio during the October 2003 superstorm. The same as the red trace of Figure 3e. (b) The Z component of the magnetic field acquired by Geotail/MGF. Vertical arrows in both panels correspond to beginning of the O^+/H^+ energy density ratio enhancement and dipolarization at 1840 UT, 1950 UT, and 2120 UT on 30 October.

red traces of the H^+ and O^+ energy densities, we noticed that the energy densities for 2130–2230 UT were smaller than those for 2050–2110 UT. This is probably caused by Geotail's motion from the inner plasma sheet to the outer plasma sheet, as can be seen in change of B_X from ~0 nT to 100–200 nT. Therefore we calculated the O^+/H^+ energy density ratio to remove the spatial effect, assuming that the ratio is spatially constant in the plasma sheet. The result is shown in Figure 3e. The O^+/H^+ energy density ratios during the quiet intervals (blue and green) were 0.1–0.5. On the other hand, the ratio was more than 1.0 in most of the storm interval (red) and had an extremely large value of 10–20 around 2230 UT, which is the largest value in the near-Earth plasma sheet ever observed by the Geotail satellite. (In the Geotail mission prior to the superstorm, the largest ratio in the near-Earth plasma sheet of $X_{GSM} = -10\ R_E$ to $0\ R_E$ and $|Y_{GSM}| \leq 8\ R_E$ was 3–4.5 during the storm with SYM-H_{min} = −187 nT on 5 October 2000.) This energy density ratio means that O^+ ions carry more than 90% of the total energy density. After the peak of 10–20, the O^+/H^+ energy density ratio started to decrease gradually. We attribute the decrease to recovery of the superstorm (Figure 3a) and a change of the Geotail location toward the dawnside (Figure 2), where the energetic ion flux becomes lower than the duskside [*Krimigis and Sarris*, 1979; *Meng et al.*, 1981; *Sarafopoulos et al.*, 2001], particularly for O^+ ions [*Nosé et al.*, 2005].

3.2. Substorm Effect on Ion Composition

[11] From a close inspection of Figure 3e we noticed that the O^+/H^+ energy density ratio during the superstorm strongly increased in a timescale of <60 min after 1840 UT, 1950 UT, and 2120 UT. In order to see if these increases are related to storm-time substorms, we examined the Geotail/MGF data. Figure 4 displays the O^+/H^+ energy density ratio during the superstorm, which is identical to that in Figures 3e, and the Z component of the magnetic field in the same interval. Vertical arrows in Figure 4 indicate times when the energy density ratio started to increase (i.e., 1840 UT, 1950 UT, and 2120 UT). We found that B_Z was gradually decreasing before the times of the vertical arrows, followed by sudden increases by ~50 nT. These are typical dipolarization signatures observed in the near-Earth plasma sheet [e.g., *Lui*, 1978]. We also examined energetic electron flux observed by the Los Alamos National Laboratory (LANL) geosynchronous satellites. The LANL-02A satellite observed electron flux enhancements at ~1840 UT and 1950 UT; the LANL-01A satellite observed flux enhancements at 1950 UT and 2120 UT (not shown here). The above results lead us to conclude that the increases of the O^+/H^+ energy density ratio were associated with storm-time substorms.

[12] It is noted that the first substorm gave rise to a rapid (~10 min) increase of the energy density ratio, while the second and third substorms were accompanied by rather gradual (~60 min) changes. The expansion phase of the second and third substorms ended around 2010 UT and 2140 UT, at which B_Z reached local maxima. Nevertheless, the energy density ratio was still increasing after these times, that is, in the recovery phase of substorms. We infer that the increases of the O^+/H^+ energy density ratio after the second and third substorms are related to an additional supply of O^+ ions from the ionosphere to the near-Earth plasma.

3.3. Ionospheric Ion Outflow Observed by IMAGE/LENA

[13] We examined the IMAGE/LENA data to test the above idea that ionospheric ion outflow took place at the second and third substorms. Figures 5a and 5b show the orbit of the IMAGE satellite for the period of 1700 UT on 30 October to 0200 UT on 31 October in the X_{GSM}-Y_{GSM} and X_{GSM}-Z_{GSM} planes. Dots and triangles indicate the satellite locations at 1-hour intervals and at the substorm onsets, respectively. Figure 5c displays the IMAGE/LENA spectrogram for the storm interval. The vertical axis gives a spin angle relative to the Earth (i.e., an Earth-centered azimuth). Two white lines running around 0° represent angular extent of the Earth. A bright yellow/red line starting from ~180° and drifting across the spectrogram is "Sun pulse," which directs toward the Sun and is caused by the charge exchange process of solar wind particles in the magnetosheath [*Collier et al.*, 2001]. A very high emission (red) around the end of 30 October is considered to be caused by radiation belt particles.

[14] Red arrows in Figure 5c indicate the onset times of the substorms which were described in the previous subsection. At the second and third substorm onsets (at 1950 UT and 2120 UT), emission of neutral atom was enhanced around the Earth (i.e., around spin angle of ~0°), indicating a flux enhancement of ionospheric ions flowing out from the Earth. Although it is difficult to identify the ion composition of the outflow with the LENA data, we suppose that O^+ ions were dominant in this outflow because the DE-1 measurements of ionospheric ion outflow revealed that the O^+ flux at energies of 10 eV to a few tens of keV becomes larger than the H^+ flux during geomagnetically active periods [*Yau et al.*, 1985; *Chappell et al.*, 1987]. In Figure 5d we plotted the LENA count data averaged over the Earth-centered azimuth of −44° to 44° (thin line) along with the Geotail observation of the O^+/H^+ energy density

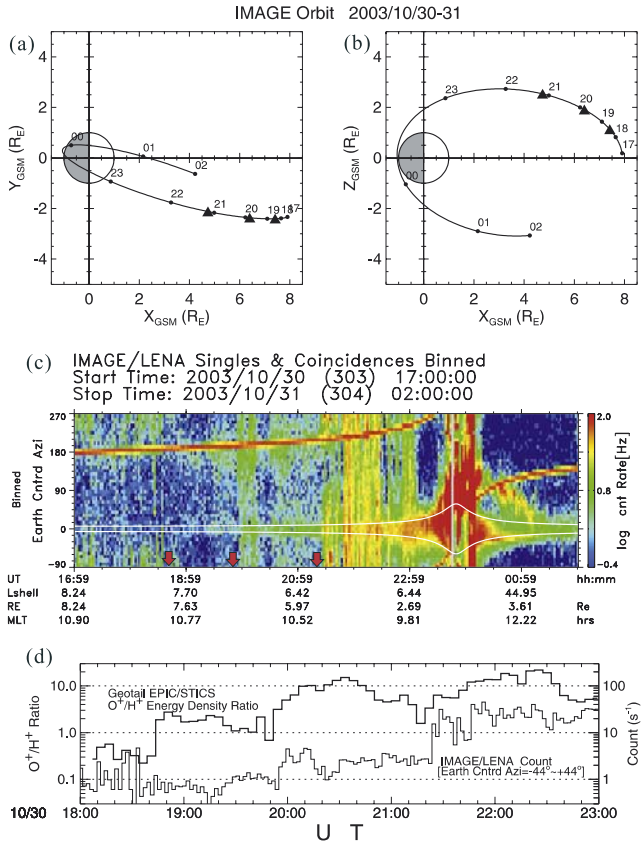

Figure 5. (a) Orbits of the IMAGE satellite in the X_{GSM}-Y_{GSM} plane for the storm interval. Dots and triangles indicate the satellite locations at 1-hour intervals and at the substorm onsets, respectively. (b) The same as Figure 5b except for the X_{GSM}-Z_{GSM} plane. (c) The IMAGE/LENA spectrogram for the storm interval with the horizontal axis of time and the vertical axis of a spin angle relative to the Earth. The count rate of neutral atom is color-coded. Two white lines running around 0° represent angular extent of the Earth. Red arrows indicate the onset times of the substorms. (d) The LENA cound data averaged over the Earth-centered azimuth of −44° to 44° (thin line) and the Geotail observation of the O^+/H^+ ratio which is the same as that in Figures 3e and 4a (thick line).

ratio (thick line) for 1800–2300 UT on 30 October. It seems that the enhancements of the neutral atom emission were delayed against the enhancements of the O^+/H^+ ratio by ≤5 min. Since 1 keV oxygen atoms have a speed of ∼110 km/s, it takes about 5 min for them to travel ∼5 R_E from the source (i.e., the site where charge exchange took place) to the IMAGE satellite, suggesting that ionospheric ion outflow was enhanced at almost the same time as the second and third substorms. These observational results support our idea. We also found that emission of neutral atoms around the Sun pulse increased and spread over wider spin angles at the same time. Such variations of emission have been studied by *Taguchi et al.* [2004], who concluded that they are caused by compression of the magnetosphere during high solar wind dynamic pressure. This implies the concurrence of ionospheric ion outflow and solar wind dynamic pressure enhancement, which is consistent with results by *Moore et al.* [1999], *Elliott et al.* [2001], *Fuselier et al.* [2002], and *Cully et al.* [2003]. Unfortunately, we could not directly confirm the implication, because solar wind density values measured by the Advanced Composition Explorer (ACE) satellite are uncertain on 30 October and their time resolution is ∼33 min [*Skoug et al.*, 2004]. For the first substorm at 1840 UT, there was no clear enhancement of emission around the spin angle of 0°. The absence of emission enhancement does not necessarily mean an absence of ion outflow from the ionosphere because the IMAGE satellite was located near the geomagnetic equatorial plane (geomagnetic latitude of ∼9°) at 1840 UT (Figure 5b). At such low geomagnetic latitudes, it is expected that neutral atoms created by charge exchange with outflowing ionospheric ions, which have the field-aligned pitch angle distribution at altitude higher than 6000 km [*Gorney et al.*, 1981; *Yau et al.*, 1984], are difficult to detect.

4. Discussion

4.1. Dynamics of O^+ Ions

[15] From the Geotail/EPIC/STICS observations, we have found that the O^+/H^+ energy density ratio during the superstorm was noticeably enhanced at three substorm onsets of 1840 UT, 1950 UT, and 2120 UT (Figure 4). According to *Delcourt et al.* [1990], *Sánchez et al.* [1993], and *Nosé et al.* [2000], substorms can accelerate ions in a mass-dependent way, resulting in more energization of O^+ ions than H^+ ions. We consider that the ion acceleration by substorms is one of the important processes for the observed O^+/H^+ enhancement during the October 2003 superstorm. However, it is worth noting here that there are a few studies reporting that substorms are less essential for ion composition change [*Nosé et al.*, 2001, 2003]. These studies have examined the recovery phase of moderate storms (Dst ∼ −140 nT) or the main phase of weak storms (SYM-H ∼ −50 nT); thus we think that the results of these studies are not the case for the main phase of the superstorm analyzed in the present study.

[16] After the second and third substorm onsets, the energy density ratio continued to increase for about ∼1 hour even in the substorm recovery phase. The IMAGE/LENA data showed that neutral atoms coming from the Earth were increased at these substorm onsets, implying flux enhancement of ionospheric ion outflow. A large number of numerical simulations have been conducted to track such ions after flowing from the ionosphere [e.g., *Cladis*, 1986, 1988; *Cladis and Francis*, 1992; *Delcourt et al.*, 1999; *Chappell et al.*, 2000]. They found that most of these ionospheric ions travel through the geomagnetic lobe and then drift into the plasma sheet within less than 1 hour to 2 hours. *Cladis* [1986] revealed that the transit time from the ionosphere to the plasma sheet becomes shorter as the convection electric field becomes large. The convection electric field during the superstorm was expected to be so large that the transit time was as short as <1 hour. This is consistent with the observed timescale of the O^+/H^+ energy density ratio increase (Figure 3e and Figure 4a). Therefore we consider that the additional supply of ionospheric ions to the plasma sheet was another important process for the ion composition change during the October 2003 superstorm.

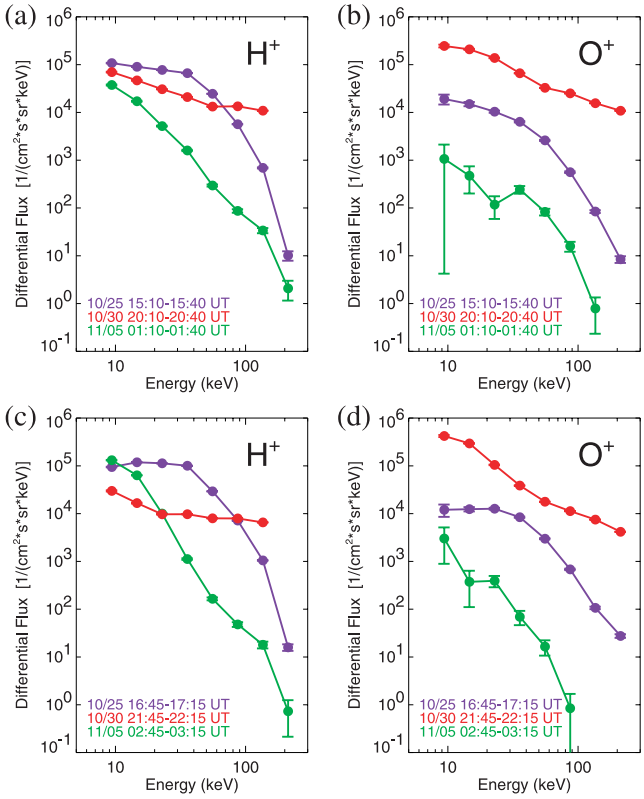

Figure 6. (a) Geotail observations of energy spectra of H^+ ions for 1510–1540 UT on 25 October (blue), 2010–2040 UT on 30 October (red), and 0110–0140 UT on 5 November (green). (b) The same as Figure 6a except for O^+ ions. (c) H^+ energy spectra for 1645–1715 UT on 25 October (blue), 2145–2215 UT on 30 October (red), and 0245–0315 UT on 5 November (green). (d) The same as Figure 6c except for O^+ ions.

[17] Figures 6a and 6b show Geotail observations of energy spectra of H^+ and O^+ for 30 min intervals after the second substorm (2010–2040 UT on 30 October, shown in red) and of two corresponding quiet intervals (1510–1540 UT on 25 October and 0110–0140 UT on 5 November, shown in blue and green). These spectra were obtained in almost the same areas of (X_{GSM}, Y_{GSM}) ~ (−8.5, 0.5) R_E (Figure 2). Figures 6c and 6d display energy spectra for the third substorm and two quiet intervals (2145–2215 UT on 30 October, shown in red; 1645–1715 UT on 25 October, shown in blue; 0245–0315 UT on 5 November, shown in green) in the area of (X_{GSM}, Y_{GSM}) ~ (−8.5, −2) R_E. From Figures 6a and 6c we found that the H^+ spectrum during the superstorm becomes harder than those during the quiet intervals. However, the O^+ spectrum during the superstorm shifts to higher flux overall as well as hardening (Figures 6b and 6d). These spectrum changes suggest that H^+ experienced acceleration during the superstorm, while O^+ experienced both acceleration and increases in number density during the superstorm. The density increases of O^+ ions in the plasma sheet agree with the LENA observations.

4.2. Estimation of Ring Current Ion Composition

[18] There are no direct measurements of differential flux of energetic O^+ ions in the inner magnetosphere for this superstorm. Using the Geotail data obtained in the near-Earth plasma sheet, we intend to estimate the O^+/H^+ energy density ratio in the ring current during the intense storm. Figure 7 summarizes the O^+/H^+ energy density ratios in the ring current and the near-Earth plasma sheet which were reported by previous studies. (This figure is reproduced from Plate 2 of *Nosé et al.* [2005] with some minor modifications.) Open circles show the O^+/H^+ energy density ratios in the ring current region observed by the AMPTE/CCE or CRRES satellites. Circles in the left part of a vertical dashed line mean observations at quiet intervals. A vertical or horizontal line is a range of the energy density ratio or a range of the Dst index derived from a statistical analysis. Numbers 1–8 next to the circles indicate references appearing at the bottom right corner of the figure. Horizontal thick arrows show the O^+/H^+ energy density ratios in the near-Earth plasma sheet (magnetic local time of 1800–0600 hour and radial distance of 8–15 R_E) obtained by the 8.4-year Geotail/EPIC data [*Nosé et al.*, 2005]. In both the ring current and the near-Earth plasma sheet, the energy density ratio increases as the Dst (or SYM-H) index decreases. We found that the O^+/H^+ energy density ratio in the ring current is very similar to that in the near-Earth plasma sheet.

[19] We overplotted the peak value of the O^+/H^+ energy density ratio for this superstorm with a filled circle in Figure 7. The filled circle seems to follow the Dst (or SYM-H) dependence of the energy density ratio expected from the previous results, suggesting that the ring current ion composition is nearly equivalent to the plasma sheet ion composition even for the superstorm. Therefore we can reasonably estimate the O^+/H^+ energy density ratio in the ring current to be 10–20 for the October 2003 superstorm.

5. Conclusions

[20] The Geotail/EPIC/STICS and IMAGE/LENA data were used to study dynamics of O^+ ions during the October

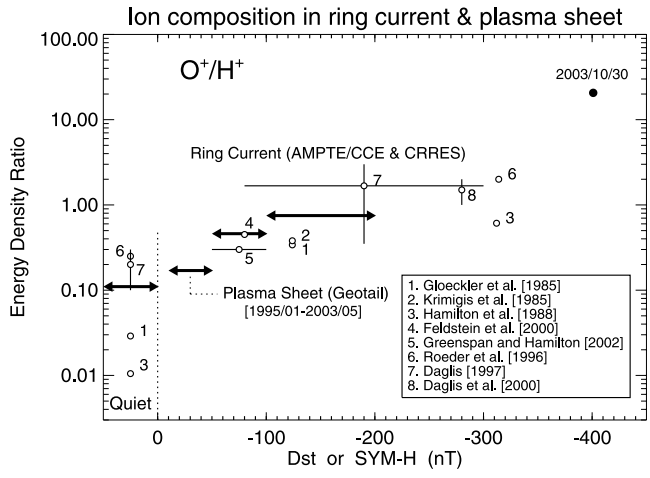

Figure 7. Summary of the O^+/H^+ energy density ratio in the ring current and the plasma sheet. Open circles represent the ratio in the ring current reported by previous studies, whose references are shown with numbers 1–8. Horizontal arrows show the Geotail results for the plasma sheet by *Nosé et al.* [2005]. The result of the October 2003 superstorm is shown with a filled circle.

2003 superstorm. We found the following results: (1) The H^+ energy density in the near-Earth plasma sheet during the superstorm was almost similar to those in the quiet times (1–10 keV cm^{-3}), while the O^+ energy density in the near-Earth plasma sheet showed a large difference between the quiet times (0.05–3 keV cm^{-3}) and the superstorm ($\sim$100 keV cm^{-3}). (2) The O^+/H^+ energy density ratio was found to reach 10–20 near the storm maximum, which is the largest ratio in the near-Earth plasma sheet ever observed by Geotail. (3) The O^+/H^+ energy density enhancements were related to substorm onsets which occurred at 1840 UT, 1950 UT, and 2120 UT on 30 October. (4) The O^+ energy spectrum during the superstorm showed both hardening and overall shift to higher flux. (5) When the second and third substorms are initiated, emissions of neutral atoms created from charge exchange with outflowing ionospheric ions are enhanced. Result 3 suggests that storm-time substorms played an important role in the increase of the O^+/H^+ energy density ratio during the October 2003 superstorm. In addition, from results 4 and 5 we found that a supply of extra O^+ ions from the ionosphere to the plasma sheet is also essential to the observed O^+/H^+ energy density ratio changes during the superstorm.

[21] We compared the ion composition changes between the ring current and the near-Earth plasma sheet, using results reported by previous studies. The comparison revealed that the ring current ion composition is similar to the plasma sheet ion composition. Thus the result 2 above leads us to assess the O^+/H^+ energy density ratio in the ring current at 10–20 for the October 2003 superstorm.

[22] **Acknowledgments.** We thank D. J. Williams and S. R. Nylund for their help in processing the Geotail/EPIC data. The SYM-H index was provided by T. Iyemori at WDC for Geomagnetism, Kyoto. The Geotail/MGF data were supplied by T. Nagai. The energetic electron data from the LANL-01A and LANL-02A satellites were provided by G. Reeves. Thanks are also due to S. Ohtani, P. C. Brandt, and Q.-G. Zong for their helpful comments. This work was supported by the Sumitomo Foundation (grant 030677) and the Atmospheric Science Division of National Science Foundation (grant ATM-0000255).

[23] Arthur Richmond thanks H. A. Elliott and Dimitrios V. Sarafopoulos for their assistance in evaluating this paper.

References

Burch, J. L. (2000), IMAGE mission overview, *Space Sci. Rev.*, *91*, 1–14.

Chappell, C. R., T. E. Moore, and J. H. Waite Jr. (1987), The ionosphere as a fully adequate source of plasma for the Earth's magnetosphere, *J. Geophys. Res.*, *92*, 5896–5910.

Chappell, C. R., B. L. Giles, T. E. Moore, D. C. Delcourt, P. D. Craven, and M. O. Chandler (2000), The adequacy of the ionospheric source in supplying magnetospheric plasma, *J. Atmos. Sol. Terr. Phys.*, *62*, 421–436.

Cladis, J. B. (1986), Parallel acceleration and transport of ions from polar ionosphere to plasma sheet, *Geophys. Res. Lett.*, *13*, 893–896.

Cladis, J. B. (1988), Transport of ionospheric ions in the magnetosphere: Theory and observations, *Adv. Space Res.*, *8*, (8)165–(8)173.

Cladis, J. B., and W. E. Francis (1992), Distribution in magnetotail of O+ ions from cusp/cleft ionosphere: A possible substorm trigger, *J. Geophys. Res.*, *97*, 123–130.

Collier, M. R., et al. (2001), Observations of neutral atoms from the solar wind, *J. Geophys. Res.*, *106*, 24,893–24,906.

Cully, C. M., E. F. Donovan, A. W. Yau, and G. G. Arkos (2003), Akebono/Suprathermal Mass Spectrometer observations of low-energy ion outflow: Dependence on magnetic activity and solar wind conditions, *J. Geophys. Res.*, *108*(A2), 1093, doi:10.1029/2001JA009200.

Daglis, I. A. (1997), The role of magnetosphere-ionosphere coupling in magnetic storm dynamics, in *Magnetic Storms*, *Geophys. Monogr. Ser.*, vol. 98, edited by B. T. Tsurutani et al., pp. 107–116, AGU, Washington, D. C.

Daglis, I. A., Y. Kamide, C. Mouikis, G. D. Reeves, E. T. Sarris, K. Shiokawa, and B. Wilken (2000), "Fine structure" of the storm-substorm relationship: Ion injections during Dst decrease, *Adv. Space Res.*, *25*, 2369–2372.

Delcourt, D. C., J. A. Sauvaud, and A. Pedersen (1990), Dynamics of single-particle orbits during substorm expansion phase, *J. Geophys. Res.*, *95*, 20,853–20,865.

Delcourt, D. C., N. Dubouloz, J.-A. Sauvard, and M. Malingre (1999), On the origin of sporadic keV ion injections observed by Interball-Auroral during the expansion phase of a substorm, *J. Geophys. Res.*, *104*, 24,929–24,937.

Elliott, H. A., R. H. Comfort, P. D. Craven, M. O. Chandler, and T. E. Moore (2001), Solar wind influence on the oxygen content of ion outflow in the high-latitude polar cap during solar minimum conditions, *J. Geophys. Res.*, *106*, 6067–6084.

Feldstein, Y. I., L. A. Dremukhina, U. Mall, and J. Woch (2000), On the two-phase decay of the Dst-variation, *Geophys. Res. Lett.*, *27*, 2813–2816.

Fuselier, S. A., H. L. Collin, A. G. Ghielmetti, E. S. Claflin, T. E. Moore, M. R. Collier, H. Frey, and S. B. Mende (2002), Localized ion outflow in response to a solar wind pressure pulse, *J. Geophys. Res.*, *107*(A8), 1203, doi:10.1029/2001JA000297.

Gloeckler, G., B. Wilken, W. Studemann, F. M. Ipavich, D. Hovestadt, D. C. Hamilton, and G. Kremser (1985), First composition measurement of the bulk of the storm-time ring current (1 to 300 keV/e) with AMPTE/CCE, *Geophys. Res. Lett.*, *12*, 325–328.

Gorney, D. J., A. Clarke, D. Croley, J. Fennell, J. Luhmann, and P. Mizera (1981), The distribution of ion beams and conics below 8000 km, *J. Geophys. Res.*, *86*, 83–89.

Greenspan, M. E., and D. C. Hamilton (2002), Relative contributions of H+ and O+ to the ring current energy near magnetic storm maximum, *J. Geophys. Res.*, *107*(A4), 1043, doi:10.1029/2001JA000155.

Hamilton, D. C., G. Gloeckler, F. M. Ipavich, W. Studemann, B. Wilken, and G. Kremser (1988), Ring current development during the great geomagnetic storm of February 1986, *J. Geophys. Res.*, *93*, 14,343–14,355.

Iyemori, T., T. Araki, T. Kamei, and M. Takeda (1992), Mid-latitude geomagnetic indices ASY and SYM (Provisional) No. 1 1989, Data Anal. Center for Geomagn. and Space Magn., Kyoto Univ., Kyoto, Japan.

Khan, H., M. R. Collier, and T. E. Moore (2003), Case study of solar wind presure variations and neutral atom emissions observed IMAGE/LENA, *J. Geophys. Res.*, *108*(A12), 1422, doi:10.1029/2003JA009977.

Kokubun, S., T. Yamamoto, M. H. Acuna, K. Hayashi, K. Shiokawa, and H. Kawano (1994), The GEOTAIL magnetic field experiment, *J. Geomagn. Geoelectr.*, *46*, 7–21.

Krimigis, S. M., and E. T. Sarris (1979), Energetic particle bursts in the Earth's magnetotail, in *Dynamics of the Mangetosphere*, edited by S.-I. Akasofu, pp. 599–630, Springer, New York.

Krimigis, S. M., G. Gloeckler, R. W. McEntire, T. A. Potemra, F. L. Scarf, and E. G. Shelley (1985), Magnetic storm of September 4, 1984: A synthesis of ring current spectra and energy densities measured with AMPTE/CCE, *Geophys. Res. Lett.*, *12*, 329–332.

Lui, A. T. Y. (1978), Estimates of current changes in the geomagnetotail associated with a substorm, *Geophys. Res. Lett.*, *5*, 853–856.

Meng, C.-I., A. T. Y. Lui, S. M. Krimigis, S. Ismail, and D. J. Williams (1981), Spatial distribution of energetic particles in the distant magnetotail, *J. Geophys. Res.*, *86*, 5692–5700.

Moore, T. E., W. K. Peterson, C. T. Russell, M. O. Chandler, M. R. Collier, H. L. Collin, P. D. Craven, R. Fitzenreiter, B. L. Giles, and C. J. Pollock (1999), Ionospheric mass ejection in response to a CME, *Geophys. Res. Lett.*, *15*, 2339–2342.

Moore, T. E., et al. (2000), The low energy neutral atom imager for IMAGE, *Space Sci Rev.*, *91*, 155–195.

Nishida, A. (1994), The GEOTAIL mission, *Geophys. Res. Lett.*, *21*, 2871–2874.

Nosé, M., A. T. Y. Lui, S. Ohtani, B. H. Mauk, R. W. McEntire, D. J. Williams, T. Mukai, and K. Yumoto (2000), Acceleration of oxygen ions of ionospheric origin in the near-Earth magnetotail during substorms, *J. Geophys. Res.*, *105*, 7669–7677.

Nosé, M., S. Ohtani, K. Takahashi, A. T. Y. Lui, R. W. McEntire, D. J. Williams, S. P. Christon, and K. Yumoto (2001), Ion composition of the near-Earth plasma sheet in storm and quiet intervals: Geotail/EPIC measurements, *J. Geophys. Res.*, *106*, 8391–8403.

Nosé, M., R. W. McEntire, and S. P. Christon (2003), Change of the plasma sheet ion composition during magnetic storm development observed by the Geotail spacecraft, *J. Geophys. Res.*, *108*(A5), 1201, doi:10.1029/2002JA009660.

Nosé, M., K. Takahashi, S. Ohtani, S. P. Christon, and R. W. McEntire (2005), Dynamics of ions of ionospheric origin during magnetic storms: Their acceleration mechanism and transport path to ring current, in *Physics and Modeling of the Inner Magnetosphere*, *Geophys. Monogr. Ser.*, vol. 155, edited by T. I. Pulkkinen, N. A. Tsyganenko, and R. H. W. Friedel, AGU, Washington, D. C.

Roeder, J. L., J. F. Fennell, M. W. Chen, M. Schulz, M. Grande, and S. Livi (1996), CRRES observations of the composition of the ring current ion populations, *Adv. Space Res.*, *17*(10), 17–24.

Sánchez, E. R., B. H. Mauk, and C.-I. Meng (1993), Adiabatic vs. non-adiabatic particle distributions during convection surges, *Geophys. Res. Lett.*, *20*, 177–180.

Sarafopoulos, D. V., N. F. Sidiropoulos, E. T. Sarris, V. Lutsenko, and K. Kudela (2001), The dawn-dusk plasma sheet asymmetry of energetic particles: An Interball perspective, *J. Geophys. Res.*, *106*, 13,053–13,065.

Skoug, R. M., J. T. Gosling, J. T. Steinberg, D. J. McComas, C. W. Smith, N. F. Ness, Q. Hu, and L. F. Burlaga (2004), Extremely high speed solar wind; 29–30 October 2003, *J. Geophys. Res.*, *109*, A09102, doi:10.1029/2004JA010494.

Taguchi, S., M. R. Collier, T. E. Moore, M.-C. Fok, and H. J. Singer (2004), Response of neutral atom emissions in the low-latitude and high-latitude magnetosheath direction to the magnetopause motion under extreme solar wind conditions, *J. Geophys. Res.*, *109*, A04208, doi:10.1029/2003JA010147.

Williams, D. J., R. W. McEntire, C. Schlemm II, A. T. Y. Lui, G. Gloeckler, S. P. Christon, and F. Gliem (1994), Geotail energetic particles and ion composition instrument, *J. Geomagn. Geoelectr.*, *46*, 39–57.

Yau, A. W., B. A. Whalen, W. K. Peterson, and E. G. Shelley (1984), Distribution of upflowing ionospheric ions in the high-altitude polar cap and auroral ionosphere, *J. Geophys. Res.*, *89*, 5507–5522.

Yau, A. W., E. G. Shelley, W. K. Peterson, and L. Lenchyshyn (1985), Energetic auroral and polar ion outflow at DE 1 altitudes: Magnitude, composition, magnetic activity dependence, and long-term variations, *J. Geophys. Res.*, *90*, 8417–8432.

S. P. Christon, Focused Analysis and Research, Columbia, MD 21044, USA.

M. R. Collier and T. E. Moore, NASA Goddard Space Flight Center, Code 692, Greenbelt, MD 20771, USA.

K. Hosokawa and S. Taguchi, Department of Information and Communication Engineering, University of Electro-Communications, 1-5-1 Chofugaoka, Chofu, 182-8585 Tokyo, Japan.

R. W. McEntire, Applied Physics Laboratory, Johns Hopkins University, 11100 Johns Hopkins Road, Laurel, MD 20723-6099, USA.

M. Nosé, Data Analysis Center for Geomagnetism and Space Magnetism, Graduate School of Science, Kyoto University, Oiwake-cho, Kitashirakawa, Sakyo-ku, Kyoto 606-8502, Japan. (nose@kugi.kyoto-u.ac.jp)